Nanoscale

Accepted Manuscript

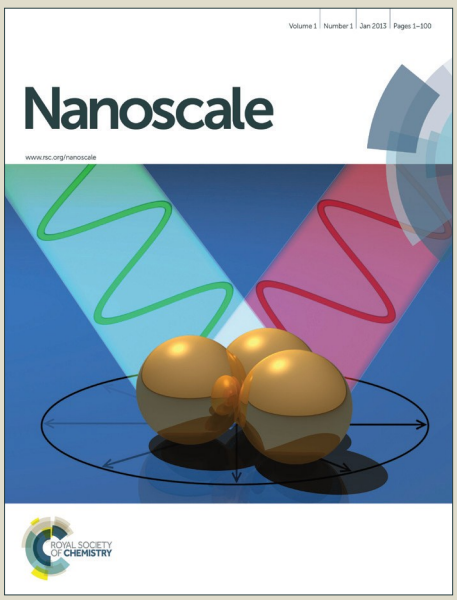

ROYAL SOCIETY OF CHEMISTRY

www.rsc.org/nanoscale

Journal Name

ARTICLE

Received 00th January 20xx,
Accepted 00th January 20xx

DOI: 10.1039/x0xx00000x

www.rsc.org/

Simultaneous Tunable Structure and Composition of PtAg Alloyed Nanocrystals as Superior Catalysts

Caihong Fang*‡, Jun Zhao‡, Guili Zhao, Long Kuai, and Baoyou Geng*

PtAg alloyed nanostructural catalysts were firstly prepared by co-reduction of the $AgNO_3$ and H_2PtCl_6 precursors in growth solution using a seed-mediated method. By simply changing the molar ratio of the metal precursors, the morphologies of the porous alloyed can be tuned from multipetals to multioctahedra. Simultaneously, the alloyed composition can be varied from $Pt_{76}Ag_{24}$ to $Pt_{66}Ag_{34}$. The catalytic properties of the prepared PtAg alloyed nanocrystals with tunable structure and composition were tentatively examined by chosen the reduction of 4-nitrophenol with $NaBH_4$. The reaction rate normalized to concentration of catalysts was calculated to be 318.9 $s^{-1}\cdot mol^{-1}\cdot L$ and 277.4 $s^{-1}\cdot mol^{-1}\cdot L$ for $Pt_{70}Ag_{30}$ and $Pt_{66}Ag_{34}$ porous catalysts, which is much higher that the pure porous Pt catalysts. Moreover, PtAg nanostructures also can serve as efficient electrocatalysts toward the methanol oxidation reaction, especially for $Pt_{70}Ag_{30}$ and $Pt_{66}Ag_{34}$ porous nanocrystals. The electrocatalytic activity and the durability were both highly enhanced compared to the commercial Pt/C catalyst. In addition, we also investigated the enhancement mechanism.

1. Introduction

Platinum nanocrystals (NCs) have been extensively investigated in environmental and energy applications, such as fuel cells, sensors, and *et al*, owing to their distinct catalytic properties[1,2]. Over the past decades, a great deal of effort has been devoted to enhancing the catalytic activity of Pt NCs. However, the high cost and low abundance of metallic Pt becomes a major barrier for its large-scale commercial applications. Researchers therefore actively developed many strategies to improve their catalytic performances in order to increase their utilization efficiency and thereby reduce Pt loading in catalysts. Besides the size, it has been recognized that the catalytic performances of the metal NCs are highly dependent on their shapes[3–5]. For example, Lou co-works have demonstrated Pt nanoframes with curvature surfaces show much higher electrocatalytic properties than cubic Pt and commercial Pt nanoparticles[6]. From the application view, various Pt NCs have therefore been prepared, such as Pt nanowires, Pt nanocubes, Pt octahedra, Pt multipods, Pt tetrahexahedron, and so forth[7–11]. Noticeably, among those above morphologies, porous metal nanostructures, as an excellent option, provide much larger surface area and thus have more active sites for catalytic reactions[12,13]. Furthermore, the interconnected structures can efficiently suppress the Ostwald ripening effects and result in their high durability [14]. Many research works have therefore focused on the synthesis and applications of porous metal NCs[15]. On the other hand, Pt-based bimetallic or multimetallic NCs, including Janus, core/shell, or alloy, have been used to replace pure Pt[1,16 ,17]. Among them, alloyed NCs is the most effective way[18,19]. Huang's prepared {111}-terminated icosahedral and octahedral Pt_3Cu NCs with high density of twin defects. Both of them exhibit enhanced electrocatalytic activities toward methanol oxidation reaction (MOR) and oxygen reduction reaction relative to commercial Pt/C[20]. Li *et al* reported dealloying process using nanocrystalline alloys as precursors to synthesize porous PtNi nanostructures. The electrocatalytic tests show that PtNi porous nanostructures exhibit superior catalytic properties[21]. PtAg alloyed NCs with different various shapes, an example in the successful development of alloyed metal NCs in recent years, also have been investigated[22–24]. Take octahedral PtAg alloyed NCs as an example, they have been proved to be an effective anodic catalyst in direct methanol fuel cells[25]. On the basis of the tremendous published works, it has been recognized that the introduction of other metals can not only decrease the required amount of

[a] College of Chemistry and Materials Science, The Key Laboratory of Functional Molecular Solids, Ministry of Education, Anhui Laboratory of Molecular-Based Materials, Anhui Normal University Wuhu in Anhui Province 241000 (China)
E-mail:chfang@mail.ahnu.edu.cn
‡These authors contributed equally
Electronic Supplementary Information (ESI) available: See
DOI: 10.1039/x0xx00000x

Pt but also can modify the electronic structures and crystallographic of Pt, which lead to the enhancement of their catalytic properties[26]. Thus, the performances of Pt-based alloyed NCs also can further be enhanced by properly engineering their composition of the NCs involved[27].

Herein, we successfully combined together the benefits of shape and composition control of metal alloyed NCs and demonstrated a facile seed-mediated method to prepare monodispersed PtAg alloyed NCs with porous nanostructures. By employing Pt nanoparticles as seeds, the mixture of $AgNO_3$ and H_2PtCl_6 as precursors, porous PtAg alloyed NCs can be easily prepared at room temperature. Silver ions serve as both the shape-directing agents and the composition manipulator. Controllable Pt/Ag atomic ratios at the range of 1.94 ($Pt_{66}Ag_{34}$) to 3.17 ($Pt_{76}Ag_{24}$) are successfully achieved by just simply varying the ratios of H_2PtCl_6 to $AgNO_3$ added into growth solution. Most importantly, the synthesized PtAg alloyed NCs simultaneously involve an interesting fine-structures evolution. The morphologies display a branched structure with a round corners and a rough surface when $AgNO_3$ was presented at a low concentration in growth solution. Interestingly, the "round corners and rough surface" gradually grown into sharp octahedra as the concentration of $AgNO_3$ increasing, resulting in a facile porous morphology that is formed by several PtAg octahedral NCs. To our best knowledge, this is the first work that can obtain such porous nanostructures and simultaneously change the composition and the shape of porous metal NCs. Furthermore, we also evaluated the catalytic properties in the reduction of 4-nitrophenol (4-NP) by $NaBH_4$ and the electrocatalytic performances toward MOR using PtAg alloyed NCs as catalysts. PtAg alloyed nanostructures exhibit excellent catalytic activities toward the reduction of 4-NP. Moreover, the porous PtAg NCs, exhibits strikingly high catalytic activity. Especially, the specific and mass activities for $Pt_{76}Ag_{24}$ catalysts were both greatly enhanced relative to commercial Pt/C catalysts.

2. Results and discussion

2.1 Materials characterizations

The porous PtAg NCs were prepared using a seed-mediated method. In a typical process, Pt nanoparticles with a size of 2.5 ± 0.2 nm (Fig. S1) served as seeds which were prepared through the reduction of H_2PtCl_6 with ice-cold $NaBH_4$ in aqueous cetyltrimethylammonium bromide (CTAB) solution. The as-prepared seed solutions were injected into the growth solution prepared by sequential addition of H_2PtCl_6, $AgNO_3$, HCl, and ascorbic acid into aqueous CTAB. PtAg alloyed NCs can be grown after left the above homogeneous mixture undisturbed for 4 days. During the whole growth process, CTAB was used as surfactant that can prevent aggregation of our products.

The porous PtAg alloyed NCs are displayed in Fig. 1a–f, together with their structural characterization results. Scanning electron microscopy (SEM) imagies (Fig. 1a, c, and e) indicate that all of the obtained products under different ratios of $AgNO_3$ to H_2PtCl_6 have a well-defined and uniform shape. Transmission electron microscopy (TEM) characterizations give more clear images. The NCs obtained under the ratio of 1:16.5 exhibit branched porous nanostructures. The outer shape shows a quasi-spherical morphology with an average outer size of 38.5 ± 2.0 nm (Fig. 1b). It is remarkable that such porous NCs (named multipetals) have round corners and rough surface on each branch. The branches inherit the petal-like structures even the ratio was increased to 1:6.60 (Fig. S2a). From the TEM images, it is clearly that the round corners gradually grown into sharp corners as the ratio was carefully changed to 1:3.30 (Fig. S2b). After the ratio of $AgNO_3$ to H_2PtCl_6 was further increased to 1:1.65, the outer shape of the alloyed NCs shows octahedra-like morphologies (named porous-octahedra, Fig. 1d). Some of the round corners in multipetals transfer to sharp corners. It should be noticed that there are still part of nanopetals with round corners in the obtained nanostructures. The outer size is also grown into 79.2 ± 4.2 nm measured from two sharp tips in the across arc position. To our surprise, the multinpetals can evolve into a new type of branched structures when the ratio of $AgNO_3$ to H_2PtCl_6 was increased to 1:0.66. As shown in Fig. 1f, the NCs maintain the branched structures from the multipetals. However, almost 100% of their branches transfer to sharp corners and display an octahedral shape. The outer morphology grows into multioctahedra. The edge length of each octahedron was measured to be 8.1 ± 1.2 nm.

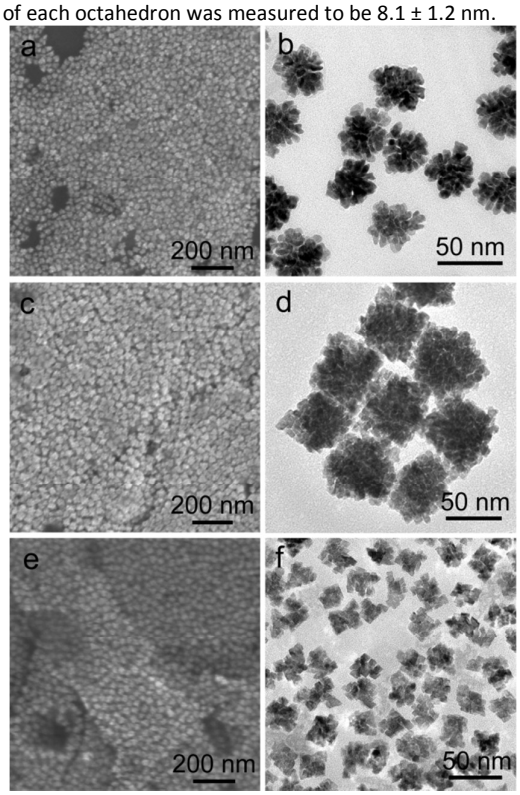

Fig. 1 Porous PtAg alloyed NCs produced by varying the ratios of H_2PtCl_6 to $AgNO_3$ in growth solution. (a, c, and e) SEM images of the porous PtAg alloyed NCs. (b, d, and f) TEM images of the corresponding porous nanostructure samples. The ratios of $AgNO_3$ to H_2PtCl_6 in growth solution were controlled to be 1:16.5, 1:1.65, and 1:0.66, respectively.

Fig. 2a is the X-ray diffraction (XRD) patterns taken on the as-prepared porous nanostructures. Three prominent peaks

present in all of the three samples, which can be indexed as a cubic structures with the peak positions located between the pure Pt and Ag diffraction patterns, respectively. These results strongly reveal the formation of alloyed NCs. The X-ray photocopy (XPS) survey spectra were also performed to explore the surface state and interaction of Pt and Ag. Fig. 2b is the typical results of as-synthesized porous-octahedra NCs. The characteristic Pt 4f displays two strong peaks at 70.7 eV (Pt $4f_{7/2}$) and 74.0 eV (Pt $4f_{5/2}$), demonstrating Pt dominantly exists in metallic Pt^0 state. In addition, the XPS peaks of metallic Ag^0 state located at 367.45 eV and 373.45 eV is assigned to Ag $3d_{5/2}$ and Ag $3d_{3/2}$, respectively. The binding energy of Ag^0 exhibits a negative shift compared to the pure monometallic Ag, which is ascribed to the charge transfer phenomenon in bimetallic or multimetallic nanostructures[28,29]. It has been proved by density functional theory calculations that the electrons transfer from metal atoms can cause binding energy decrease, revealed from XPS spectrum[30]. Herein, we therefore confirmed that the electrons around Ag transfer to Pt, leading to the substantial decrease in the local electron density around Ag atoms. Such electron transfer results in the negative shift in binding energy of metallic Ag^0. The XPS spectra of the other two samples (PtAg multipetals and multioctahedra) also exhibit the similar results (Fig. S3). Furthermore, the compositions of those porous PtAg NCs were further characterized by inductively coupled plasma-atomic emission spectroscopy (ICP–AES) analysis. The three samples we as-synthesized were determined to be $Pt_{76}Ag_{24}$, $Pt_{70}Ag_{30}$, and $Pt_{66}Ag_{34}$ NCs, respectively.

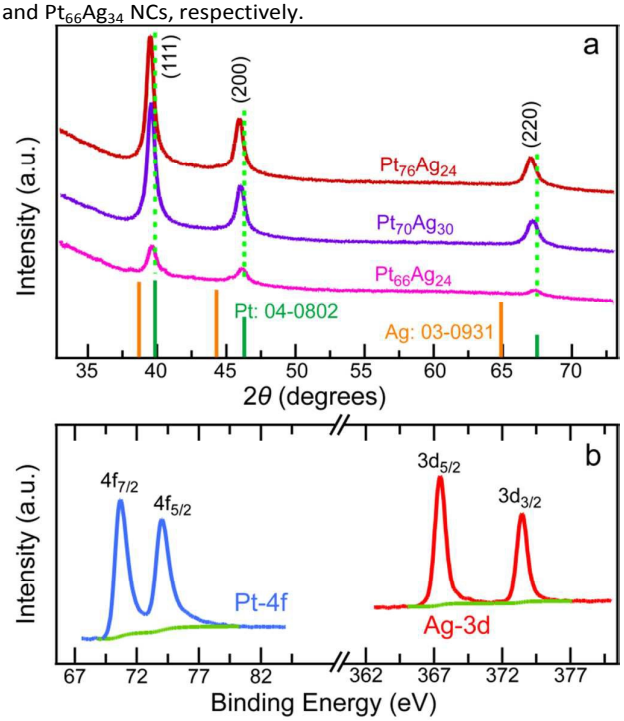

Fig. 2 (a) XRD patterns of the as-prepared porous $Pt_{76}Ag_{24}$, $Pt_{70}Ag_{30}$, and $Pt_{66}Ag_{34}$ nanostructure samples. The yellow and dark green vertical lines indicate the peak positions of pure Ag (PDF card No.: 03–0931) and Pt (PDF card No.: 04–0802), respectively. The light green dotted lines correspond to the peak position of pure Pt. (b) XPS spectra of Pt 4f and Ag 3d of the as-prepared porous-octahedra PtAg ($Pt_{70}Ag_{30}$) NCs.

PtAg alloyed NCs were further verified by high-angle annular dark-field scanning transmission electron microscopy (HAADF-STEM) imaging and high-resolution TEM (HRTEM) (Fig. 3a–f). HAADF-STEM images indicate that $Pt_{76}Ag_{24}$ NCs are porous and assume a roughly spherical shape (Fig. 3a). To more clearly reveal the detailed structure and the crystalline structures of the NCs, HRTEM and electron diffraction (ED) were acquired. The HRTEM imaging of the individual NCs further prove that the NCs is multipetal morphology (Fig. 3b). Clear lattice fringe of a entire NC with an interfringe lattice of ~0.23 nm can be observed. This interfringe lattice is corresponding to the lattice spacing of the PtAg {111} facets. ED patterns performed the entire NC display a single set of the sharp diffraction spots (Insert in Fig. 3b). HRTEM together with the ED patterns therefore unambiguous reveal that the porous NCs are single-crystalline which covered by {111} facets. These similar features are also observed in the characterizations of $Pt_{70}Ag_{30}$ and $Pt_{66}Ag_{34}$ NCs. Noticeably, it is clearly that an evolution from round multipetals to sharp multioctahedra occurs as the ratio of $AgNO_3$ to H_2PtCl_6 increasing, which are agreed well with the SEM and TEM results (Fig. 3c–f). HRTEM and ED or fast Fourier transform (FFT) patterns also confirm a high quality of single-crystalline. Moreover, the elemental mapping was acquired to reveal the elemental distributions. Fig. 3g–j display the results of the $Pt_{70}Ag_{30}$ NCs. Both Ag and Pt signals are observed, which strongly confirms the coexistence of these two elements. The complete overlapping of these two components unambiguously proves the formation of PtAg alloyed structure. The elemental mapping of the $Pt_{76}Ag_{24}$ and $Pt_{66}Ag_{34}$ NCs also exhibit the similar results, verifying the formation of alloyed NCs obtained under different ratio of $AgNO_3$ to H_2PtCl_6 (Fig. S4).

To unravel the growth mechanism of the porous PtAg alloyed NCs, we systematically performed control experiments. It is found that Ag^+ in growth solution appears to be the key for the formation of porous PtAg alloyed nanostructures. Colorless and transparent solution instead of brown solution was obtained without $AgNO_3$ in growth solution even after the reaction was carried out for over half a month (Fig. S5). We also centrifugated the resulting transparent solution at a high speed (over 12000 r/min). No precipitate can be collected at the bottom of the centrifuge tubes, further indicating that no nanostructure samples were prepared in absence of Ag^+.

In addition to Ag^+, pH value also plays a critical role. Experimentally, we found that the multioctahedra-shaped NCs can be easily grown when the pH values of the growth solution were fixed at the range of 1.98 to 2.44 (Fig. S6a–d). PtAg multipetals were obtained if the pH value were increased to the range of 3.47 to 10.82 (Fig. S6e–h). Furthermore, the NC size is readily controlled by changing the amount of seeds injected into growth solution. The average size decreases from

Journal Name

ARTICLE

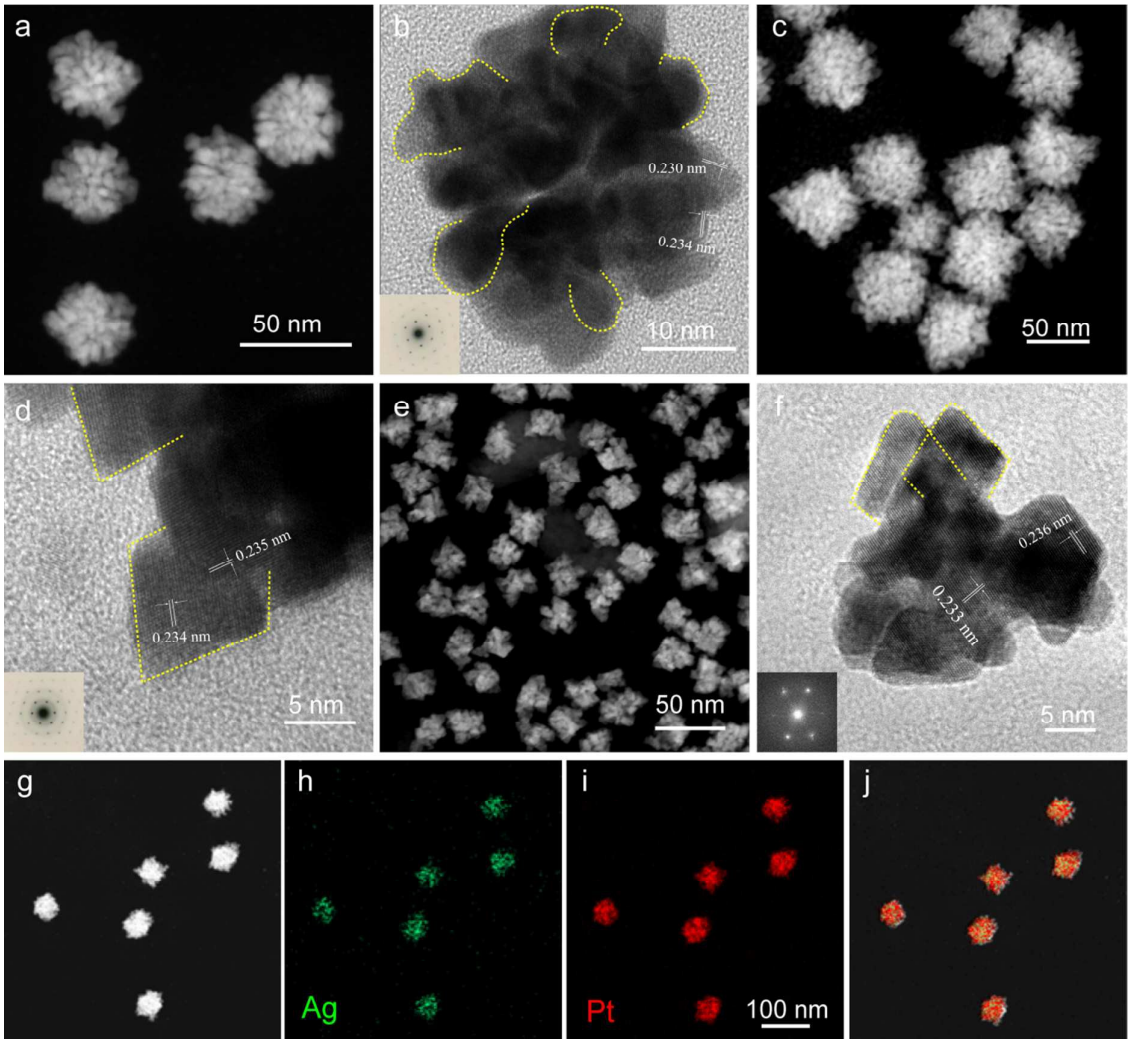

Fig. 3 Porous $Pt_{76}Ag_{24}$, $Pt_{70}Ag_{30}$, and $Pt_{66}Ag_{34}$ alloyed NC samples. (a,b) HAADF-STEM and HRTEM images of the porous $Pt_{76}Ag_{24}$ alloyed NCs, respectively. (c,d) HAADF-STEM and HRTEM images of the porous $Pt_{70}Ag_{30}$ alloyed NCs, respectively. (e,f) HAADF-STEM and HRTEM images of the porous $Pt_{66}Ag_{34}$ alloyed NCs, respectively. Inserts in b and d show the corresponding ED patterns. Insert in f is the corresponding FFT pattern. The yellow lines indicate the margin of the porous structures in b, d, and f. The scale bar in i also applies for g, h, and j.

79.2 ± 4.2 nm to 34.5 ± 2.7 nm with the quite similar porous structures as the seed volume was increased from 200 to 1000 μL (Fig. S7a–d).

Taken all the results, it is apparent that Ag^+ is essential for the formation of porous PtAg alloyed nanostructures. Moreover, the ratio of $AgNO_3$ to H_2PtCl_6 in growth solution also have very significant influence on the morphology and the composition of the alloyed NCs. Ag^+ have been intensely reported as the shape-directing agents on the basis of underpotential deposition (UPD) mechanism[31]. In our approach, Ag^+ is more reactive at room temperature in aqueous precursor solution at initial stage. Silver ions are reduced to Ag^0 and form a Ag UPD layer, which will deposit preferentially on the small-sized Pt seed nanoparticles. On the other hand, it is well established that H_2PtCl_6 in growth solution is first converted into Pt^{II} species during the synthesis of Pt NCs[32]. The formed Ag UPD layer can undergo a galvanic replace reaction with the Pt^{II} species, by which Ag^+ promote

the reduction of Pt^{II} to Pt^{0} [33]. Moreover, the oxidation etching in the presence of Br^- and O_2 [13], occurring preferentially at the sites with high energy at the surface, the porous nanostructures are thus formed. Together with the selective chemisorption of Ag^+ at the surface of Pt nanoparticles seeds induces the preferential overgrowth, producing NCs with petal or octahedral constitutions. Simultaneously, as the increase of the deposited metal Ag atoms, they will gradually mix with Pt atoms due to the small lattice mismatch of 4.1% between cubic Ag and Pt (the lattice contact of Ag and Pt is 4.08 and 3.92 nm, respectively)[25,34]. Eventually, the porous PtAg alloyed nanostructures with different fine structure and composition are formed.

2.2 Catalytic performances

The catalytic performance was tentatively evaluated in the reduction of 4-NP by $NaBH_4$. 4-NP exhibits a absorption peak at around 317 nm in neutral or acidic solution. The addition of $NaBH_4$ makes the absorption peak shift to about 400 nm due to the deprotonation of the OH group in 4-NP[35]. Such characteristic peak drops gradually in intensity if the reduction reaction is started. The reaction therefore can be monitored by measuring the absorption spectra as a function of reaction time. The peak intensity at 400 nm decreases dramatically to ~14 % of its initial intensity after $Pt_{70}Ag_{30}$ NCs were added in just 10 min, revealing the reduction of 4-NP (Fig. S8a). Additionally, we also calculated the reaction rate constant k to be 3.14×10^{-3} s^{-1} from the rate equation $\ln[C(t)/C(0)]=kt$ (Fig. S8b). Considering the catalyst mass, the reaction rate equation can be calculated as following [36]

$$\frac{dc_{(t)}}{dt} = k'[\mathrm{M}]ct \rightarrow \frac{dc_{(t)}}{dt}/[M] = k'ct$$

where ct and [M] (mol·L^{-1}) is the concentration of the 4-NP and catalysts, respectively. k' is the reaction rate normalized to concentration of catalysts. k' was calculated to be 318.9 s^{-1}·mol^{-1}·L. Accordingly, k was experimentally calculated to be 1.56×10^{-3} s^{-1}, 3.04×10^{-3} s^{-1}, 1.98×10^{-3} $s^{-1}$and k' was calculated to be 34.5 s^{-1}·mol^{-1}·L, 277.4 s^{-1}·mol^{-1}·L, and 19.8 s^{-1}·mol^{-1}·L when $Pt_{76}Ag_{24}$, $Pt_{66}Ag_{34}$ and Pt black NCs was utilized as the catalyst, respectively (Fig. S8c–h). Our findings corroborate that the PtAg alloyed nanostructures, especially for $Pt_{70}Ag_{30}$ and $Pt_{66}Ag_{34}$ NCs, exhibit much more excellent catalytic activities toward the reduction of 4-NP than that of pure porous Pt nanostructures[36] and Pt black.

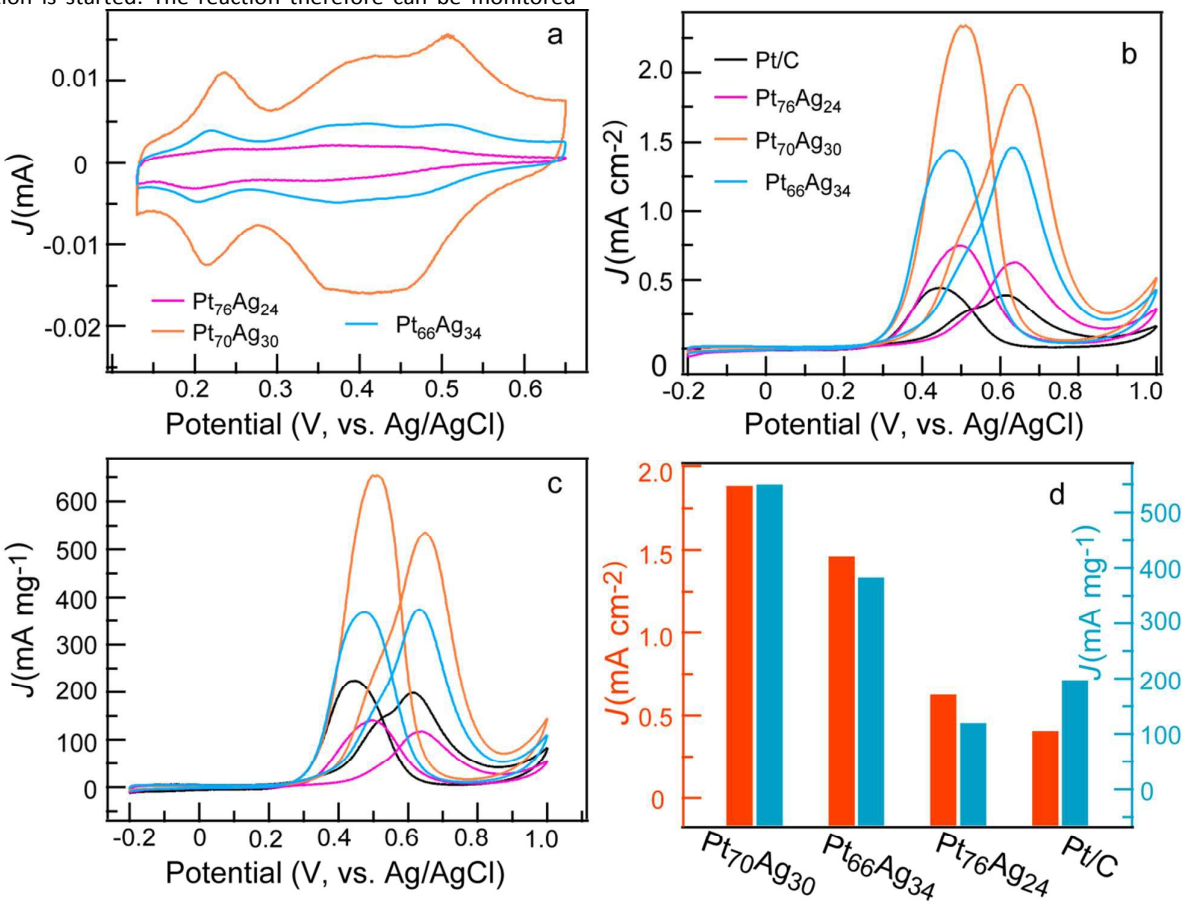

Fig. 4 (a) CV curves for $Pt_{76}Ag_{24}$, $Pt_{70}Ag_{30}$, and $Pt_{66}Ag_{34}$ NCs in N_2-saturated solution of H_2SO_4 (0.05 M) and $CuSO_4$ (0.05 M) at a scanning rate of 5 mV·s^{-1}. (b,c) Curves of specific and mass activitity normalized by ESCAs or mass of Pt for $Pt_{76}Ag_{24}$, $Pt_{70}Ag_{30}$, $Pt_{66}Ag_{34}$ NCs and commercial Pt/C in N_2-saturated solution of methanol (1.0 M) and H_2SO_4 (0.5 M) at a scanning rate of 20 mV·s^{-1}, respectively. (d) Specific and Pt-mass activities of the $Pt_{76}Ag_{24}$, $Pt_{70}Ag_{30}$, $Pt_{66}Ag_{34}$ NCs and commercial Pt/C catalysts.

Journal Name

ARTICLE

The electrocatalytic MOR properties of our as-prepared porous PtAg alloyed NCs were investigated and compared with commercial Pt/C (20 wt.% loading). We employed the Cu UPD method to estimate electrochemcial surface areas (ECSAs) of Pt-based alloyed that is much more accurate for alloyed nanostructures than hydrogen adsorption–desorption method[37]. The cyclic voltammetry (CV) curves were recorded in N_2-purged mixture of H_2SO_4 (50 mM) and $CuSO_4$ (50 mM) at a sweep rate of 5 $mV{\cdot}s^{-1}$. ECSAs were respectively calculated as 16.04 $m^2{\cdot}g^{-1}$ for $Pt_{76}Ag_{24}$, 22.67 $m^2{\cdot}g^{-1}$ for $Pt_{70}Ag_{30}$, 19.93 $m^2{\cdot}g^{-1}$ for $Pt_{66}Ag_{34}$ NCs from the CV curves (0.15 V–0.65 V) as shown in Fig. 4A. The ECSA of commercial Pt/C was calculated to be 50.89 $m^2{\cdot}g^{-1}$(Fig. S9). The electrocatalytic activity toward MOR was conducted in methanol solution (1 M) in acidic condition (H_2SO_4, 0.5 M). Obvious anodic peaks for MOR were detected in CV curves for all of the $Pt_{76}Ag_{24}$, $Pt_{70}Ag_{30}$, and $Pt_{66}Ag_{34}$ alloyed catalysts (Fig. 4b), indicating that porous alloyed nanomaterials exhibit high electrocatalytic properties. Moreover, the oxidization peaks in forward scan gradually move from 0.61 V to 0.64 V, 0.65 V, and 0.63 V when porous $Pt_{76}Ag_{24}$, $Pt_{70}Ag_{30}$, and $Pt_{66}Ag_{34}$ NCs were used instead of Pt/C. This shift in oxidation peak position give rise from alloyed effect[38], suggesting further again the formation of alloyed nanostructures. Furthermore, Pt mass activity of the $Pt_{70}Ag_{30}$, and $Pt_{66}Ag_{34}$ at 0.5 V is respectively determined to be 237 and 161.5 $mA{\cdot}mg^{-1}$, much higher than that of commercial Pt/C (128 $mA{\cdot}mg^{-1}$), strongly indicating that the electrocatalytic activities are remarkably improved (Fig. 4c). The $Pt_{76}Ag_{24}$ NCs catalysts show a mass activity of 38.4 $mA{\cdot}mg^{-1}$ to Pt/C at 0.5 V. In addition, we summarized the mass and specific activities of various catalysts for MOR by normalized the peak current intensity over the Pt loading mass or the specific area. As illustrated in Fig. 4d, it is much clearly that the mass and specific activities are significantly improved for porous $Pt_{70}Ag_{30}$ and $Pt_{66}Ag_{34}$ NCs compared to the commercial Pt/C catalysts. It should be noticed that the $Pt_{70}Ag_{30}$ NCs exhibits the highest mass and specific activity. The mass activity of $Pt_{70}Ag_{30}$ NCs are measured to be 535.8 $mA{\cdot}mg^{-1}$, 4.5 times, 1.4 times and 2.7 times higher than that of $Pt_{76}Ag_{24}$, $Pt_{66}Ag_{34}$, and commercial Pt/C, respectively. Similarly, the specific activity of $Pt_{70}Ag_{30}$ NCs is 1.91 $mA{\cdot}cm^{-2}$, which is 3.1 times, 1.3 times, and 4.9 times higher than that of $Pt_{76}Ag_{24}$, $Pt_{66}Ag_{34}$, and commercial Pt/C.

The durability of the PtAg alloyed nanostructures and the commercial Pt/C catalysts were also further tested using chronoamperometry technique. The current exponentially decay at the first stage before it reaches a pseudo steady state. Such decay is unavoidable due to the methanol concentration difference caused by diffusion on the surface of anode and the formation of the Pt oxide [22]. Clearly, the current density at pseudo steady state of $Pt_{70}Ag_{30}$ alloyed NCs is the highest in contrast to $Pt_{76}Ag_{24}$, $Pt_{66}Ag_{34}$, and Pt/C NCs. After 3000 s, the current density of $Pt_{70}Ag_{30}$ nanostructures is 0.33 $mA{\cdot}cm^{-2}$, which is 7.5 times higher than that of Pt/C, suggesting the incorporation of Ag into Pt can not only improve its electrocatalytic activity, but also enhance its stability for MOR in the presence of H_2SO_4 (Fig. 5a).

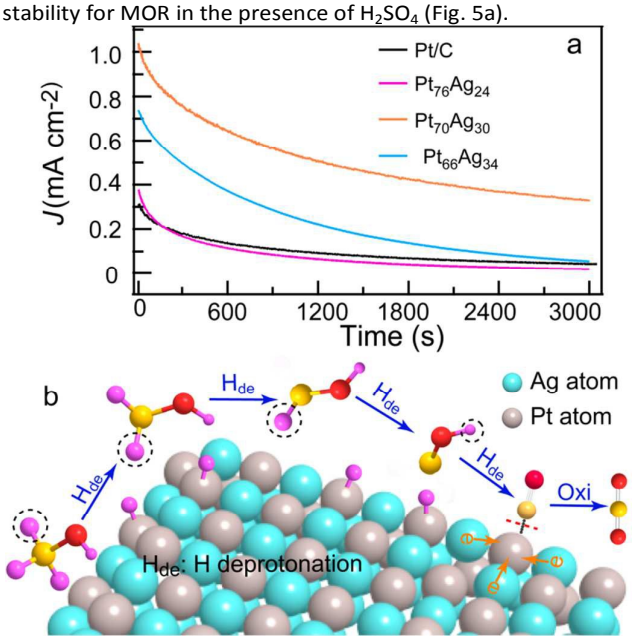

Fig. 5 (a) Chronoamperometry curves for $Pt_{76}Ag_{24}$, $Pt_{70}Ag_{30}$, and $Pt_{66}Ag_{34}$ alloyed NCs and Pt/C in the mixture of methanol (1.0 M) and H_2SO_4 (0.5 M) for 3000 s at 0.5 V. (b) Illumination of the mechanism of methanol oxidation on PtAg alloyed catalysts.

Taken together, two major changes are seen in the electrocatalytic tests. One is that the electrocatalytic performances are highly enhanced of our prepared porous PtAg alloyed NCs with different porous morphologies and compositions, especially for $Pt_{70}Ag_{30}$ and $Pt_{66}Ag_{34}$ NCs, compared to commercial Pt/C. The other is the electrocatalytic performance of porous-octahedral $Pt_{70}Ag_{30}$ alloyed NCs is higher than that of the $Pt_{66}Ag_{34}$ multioctahedral NCs. The enhancement effect can be ascribed to the following three reasons: (i) porous PtAg alloyed NCs with multipetals and multioctahedra morphologies provide abundance of edges, corners, and step atoms, which can largely increase the Pt catalytic activity towards MOR[29]. Furthermore, the fine structure of our porous alloyed NCs also is the key to enhance their performance[39]. (ii) The electronic coupling between the Ag and Pt also play a vital role[29]. (iii) The sharp-tip effect of our

porous alloyed nanostructures cause the accumulation of the negative charges on the Pt atoms at the sharp sites[40], which will benefit for the electrocatalytic enhancement. The electrocatalytic methanol oxidation reaction in acid taken Pt as catalysts can be generally divided into several steps as illustrated in Fig. 5b:

$Pt + CH_3OH \longrightarrow Pt{-}CH_2OH + Pt{-}H$ (1)

$Pt + Pt{-}CH_2OH \longrightarrow Pt_2{-}CHOH + Pt{-}H$ (2)

$Pt + Pt_2{-}CHOH \longrightarrow Pt_3{-}COH + Pt{-}H$ (3)

$Pt{-}H \longrightarrow Pt + e + H^+$ (4)

$Pt_3{-}COH \longrightarrow Pt{-}CO + Pt{-}H + e \longrightarrow Pt{-}CO + Pt$ (5)

In general case, Pt−CO will suppress the electrocatalytic activity of Pt sites. In this regard, the presence of Ag atoms in alloyed NCs can act as electron donators that transfer electrons to Pt, leading to a substantial increase in the electron density at around Pt atoms. The irreversible adsorption of CO is oxidized and therefore increases the catalytically active sites in Pt atoms. On the other hand, the coherent contact between Ag and Pt atoms in the alloyed NCs will undoubtedly decrease the surface area of the active Pt sites. The ECSAs of the PtAg alloyed nanostructures will be reduced if too many Ag atoms are introduced. The above two affects offsets with each other. That is the coupling enhanced effect will dominant if just a proper amount of Ag atoms are employed, leading to the high improvement in electrocatalytic properties of $Pt_{70}Ag_{30}$ catalysts. Otherwise, the electrocatalytic activity will be impressed if too many Ag atoms are introduced. The mass and specific activity of $Pt_{66}Ag_{34}$ NCs is therefore lower than that of $Pt_{70}Ag_{30}$ NCs. Moreover, no obvious enhancement in electrocatalytic performance of $Pt_{76}Ag_{24}$ alloyed NCs. It has been reported that the catalytic enhancement in alloyed nanocrystals is due to not only the alloyed effect, but also the sharp-tip effect[40]. Obviously, the sharp-tips effect in $Pt_{76}Ag_{24}$ multipetals is less than in the $Pt_{70}Ag_{30}$ porous-octahedra and $Pt_{66}Ag_{34}$ multioctahedra. We therefore ascribe the relative poor catalytic properties of $Pt_{76}Ag_{44}$ NCs to their less sharp-tip effect.

3. Experimental section

3.1 Synthesis of porous PtAg alloyed nanocrystals

The PtAg alloyed NCs were synthesized using a seed-mediated method. Specifically, Pt seed solution was prepared by adding a freshly prepared, ice-cold $NaBH_4$ (0.01 M, 600 μL) into a mixture of H_2PtCl_6 (0.01 M, 80 μL) and CTAB solution (0.1 M, 9.75 mL). The resulted solution was mixed by reversion and then kept at 35 ºC for at least 2 h. The growth solution was obtained by sequentially adding H_2PtCl_6 (0.01 M, 660 μL), $AgNO_3$ (0.01 M, 400 μL), HCl (1 M, 400 μL), and ascorbic acid (0.1 M, 320 μL) into aqueous CTAB (0.1 M, 9.75 mL). The pH value of the growth solution was measured to be 2.15 at the current condition. The seed solution (200 μL) was rapidly injected into the growth solution under stirring. The resultant mixture was left at 35 ºC for 4 days. The obtained alloyed NCs were centrifugated twice to remove CTAB before characterizations and use. The composition of PtAg alloyed NCs can be tuned by changing the amount of $AgNO_3$ in the growth solution. In our work, $Pt_{76}Ag_{24}$, $Pt_{70}Ag_{30}$, and $Pt_{66}Ag_{34}$ nanostructures were synthesized when 40, 400, and 1000 μL $AgNO_3$ was respectively added in growth solution.

3.2 Electrochemical measurements towards MOR

The glassy carbon electrodes (3 mm in diameter, Pine Instrument) were sequentially polished with 1 and 0.05 μm Al_2O_3 paste (mixed Al_2O_3 powder with DI water) before they were cleaned by ultrasonication. The centrifugated PtAg alloyed samples were first dispersed onto XC-72R carbon. The ink solution was then made by dispersed $Pt_{76}Ag_{24}$/C, $Pt_{70}Ag_{30}$/C, $Pt_{66}Ag_{34}$/C, or commercial Pt/C into the mixture of N,N−dimethylmethanamide (DMF) and Nafion (5 wt.%) under ultrasonication for about 10 min (for details of the exact mass of each component, see Table S1 in Supporting Information). 5−6 μL of as-prepared the ink suspension was then dropped onto the surface of modified glassy carbon disk electrode. A beaker was covered onto the working electrodes during drying procedure to control the evaporation rate. The electrodes were then dried naturally at room temperature. Herein, we should declare that the potential values in our tests are referenced to Ag/AgCl saturated electrodes.

We employed a three electrodes system where an Ag/AgCl electrode and a Pt mesh were employed as a reference and counter electrode, respectively. The potential values in this work are therefore respect to the Ag/AgCl electrode. Prior to each electrochemical measurement, the related solution was purged N_2 for about 25 min to achieve N_2-saturated solution. Chronoamperometry curves were tested by fixed the potential at 0.5 V.

3.3 Characterizations

SEM images were obtained on an FESEM Hitachi S4800 microscope. TEM imaging was carried out on an FEI Tecnai G2 20 microscope operating at 200 kV. XRD patterns were acquired on Philips X' Pert system equipped with Cu K α radiation (λ= 1.5419 Å, scanning rate = 1.0°/min). The HRTEM were taken on Tecnai G2 20 S-TWIN operated at 200 kV accelerating voltage. XPS was measured on a Thermo ESCALAB 250 system. Elemental mapping and HAADF-STEM imaging were carried out on an JEOL−2010 microscope equipped with an energy-dispersive X-ray analysis system. The absorption spectra of the solution were acquired on a Hitachi U-3900 with cuvettes with a 1.0-cm optical path length. All of the CV and chronoamperometry curves were conducted on an electrochemical workstation (Zennium, ZAHNER). ICP-AES was conducted by Optima 5300DV (Perkin Elmer). The pH values of the growth solutions were measured on PHSJ-4F (Shanghai INESA&Scientific Instrument Co. LTD).

4. Conclusions

In summary, we have demonstrated a facile seed-mediated method to prepared porous PtAg alloyed NCs. The fine structures of the alloyed NCs can be tuned from multipetals to multioctahedra by simply changing the ratios of $AgNO_3$ to

H_2PtCl_6 in growth solution. Simultaneously, the atom ratios of Pt/Ag in alloyed NCs can also be varied from 3.17 ($Pt_{76}Ag_{24}$ NCs) to 1.94 ($Pt_{66}Ag_{34}$ NCs). Electrocatalytic measurements reveal that the PtAg alloyed NCs, especially for $Pt_{70}Ag_{30}$ NCs, exhibit high activity and stability in the reduction of 4-NP by $NaBH_4$ and the electrocatalytic performances toward MOR. Therefore, we simultaneously address two key challenges, morphology and chemical composition, in improving the catalytic performance of alloyed metal NCs. We thus believe that our work will inspire new insight into rationally tailoring the morphology and chemical composition of Pt-based alloyed NCs to improve their performance in direct methanol fuel cells.

Acknowledgements

This research was financially supported by National Natural Foundation of China (21501005 and 21271009), Anhui Provincial National Science Foundation (1508085SQB199), and Natural Science Foundation of Anhui Provincial Education Department (KJ2015A029).

Notes

The authors declare no competing financial interest.

References

1 H. Zhang, M. S. Jin and Y. N. Xia, *Chem. Soc. Rev*. **2012**, *41*, 8035.
2 A. C. Chen and P. Holt-Hindle, *Chem. Rev*. **2010**, *110*, 3767.
3 J. Y. Chen, B. Lim, E. P. Lee and Y. N. Xia, *Nano Today* **2009**, *4*, 81.
4 A. Mohanty, N. Gary and R. C. Jin, *Angew. Chem. Int. Ed*. **2010**, *49*, 4962.
5 S. H. Sun, D. Q. Yang, D. Villers, G. X. Zhang, E. Sacher and J.-P. Dodelet, *Adv. Mater.* **2008**, *20*, 571–574.
6 B. Y. Xia, H. B. Wu, X. Wang and X. W. Lou, *Angew. Chem. Int. Ed*. **2013**, *52*, 12337–12340.
7 Y. J. Kang, J. B. Pyo, X. C. Ye, R. E. Diaz, T. R. Gordon, E. A. Stach and C. B. Murray, *ACS Nano* **2013**, *7*, 645.
8 R. P. Li, K. F. Bian, Y. X. Wang, H. W. Xu, J. A. Hollingsworth, T. Hanrath, J. Y. Fang and Z. W. Wang, *Nano Lett.* **2015**, *15*, 6254.
9 X. Q. Huang, Z. P. Zhao, Y. Chen, E. B. Zhu, M. F. Li, X. F. Duan and Y. Huang, *Energy Environ. Sci*. **2014**, *7*, 2957.
10 M. Subhramannia, K. Ramaiyan and V. K. Pillai, *Langmuir* **2008**, *24*, 3576.
11 N. Tian, Z.-Y. Zhou, S.-G. Sun, Y. Dong and Z. L. Wang, *Science* **2007**, *316*, 732.
12 B. Lim and Y. N. Xia, *Angew. Chem. Int. Ed*. **2011**, *50*, 76.
13 F. Wang, C. H. Li, L.-D. Sun, C.-H. Xu, J. F. Wang, J. C. Yu and C.-H. Yan, *Angew. Chem. Int. Ed.* **2012**, *51*, 4872–4876.
14 W. Y. Wang, D. S. Wang, X. W. Liu, Q. Peng and Y. D. Li, *Chem. Commun*. **2013**, *49*, 2903.
15 J. Ying, X.-Y. Yang, G. Tian, C. Janiak and B.-L. Su, *Nanoscale* **2014**, *6*, 13370.
16 J. P. Lai, W. X. Niu, R. Luque and G. B. Xu, *Nano Today* **2015**, *10*, 240.
17 J. W. Hong, S. W. Kang, B.-S. Choi, D. Kim, S. B. Lee and S. W. Han, *ACS Nano* **2012**, *6*, 2410.
18 Y. H. Bing, H. S. Liu, L. Zhang, D. Ghosh and J. J. Zhang, *Chem. Soc. Rev.* **2010**, *39*, 2184.
19 L. Zhang, J. W. Zhang, Q. Kuang, S. F. Xie, Z. Y. Jiang, Z. X. Xie and L. S. Zheng, *J. Am. Chem. Soc*. **2011**, *133*, 17114.
20 X. H. Sun, K. Z. Jiang, N. Zhang, S. J. Guo and X. Q. Huang, *ACS Nano* **2015**, *9*, 7634.
21 D. S. Wang, P. Zhao, and Y. D. Li, *Sci. Rep*. **2011**, *1*, 37.
22 X. Cao, N. Wang, Y. Han, C. Z. Gao, Y. Xu, M. X. Li and Y. H. Shao, *Nano Energy* **2015**, *12*, 105.
23 P. Song, L.-L. He, A.-J. Wang, L.-P. Mei, S.-X. Zhong, J.-R. Chen and J.-J. Feng, *J. Mater. Chem. A* **2015**, *3*, 5321.
24 A. A. Umar, E. Rahmi, A. Balouch, M. Y. A. Rahman, M. M. Salleh and M. Oyama, *J. Mater. Chem. A* **2014**, *2*, 17655.
25 G.-T. Fu, R.-G. Ma, X.-Q. Gao, Y. Chen, Y.-W. Tang, T.-H. Lu and J.-M. Lee, *Nanocale* **2014**, *6*, 12310.
26 K. P. Gong, D. Su and R. R. Adzic, *J. Am. Chem. Soc*. **2010**, *132*, 14364.
27 C. Chen, Y. J. Kang, Z. Y. Huo, Z. W. Zhu, W. Y. Huang, H. L. Xin, J. D. Snyder, D. G. Li, J. A. Herron, M. Mavrikakis, M. F. Chi, K. L. More, Y. D. Li, N. M. Markovic, G. A. Somorjai, P. D. Yang and V. R. Stamenkovic, *Science* **2014**, *343*, 1339.
28 X. B. Xie, G. H. Gao, S. D. Kang, T. Shibayama, Y. H. Lei, D. Y. Gao and L. T. Cai, *Adv. Mater.* **2015**, *27*, 5573.
29 H. Liu, F. Ye, Q. F. Yao, H. B. Cao, J. P. Xie, J. Y. Lee and J. Yang, *Sci Rep*. **2014**, *4*, 3969.
30 Y. Wu, D. S. Wang, G. Zhou, R. Yu, C. Chen and Y. D. Li, *J. Am. Chem. Soc.***2014**, *136*, 11594.
31 E. Herrero, L. J. Buller and H. D. Abruña, *Chem. Rev.* **2001**, *101*, 1897.
32 J. Chen, T. Herricks and Y. Xia *Angew. Chem. Int. Ed*. **2005**, *44*, 2589.
33 Y. Yu, Q. B. Zhang, J. P. Xie and J. Y. Lee, *Nat. Commun.* **2013** *4*, 1454.
34 Z. Q. Niu, D. S. Wang, R. Yu, Q. Peng and Y. D. Li, *Chem. Sci.* **2012**, *3*, 192.
35 Z. Jin, M. D. Xiao, Z. H. Bao, P. Wang and J. F. Wang, *Angew. Chem. Int. Ed*. **2012**, *51*, 6406.
36 T. Yu, J. Zeng, B. Lim and Y. N. Xia, *Adv. Mater.* **2010**, *22*, 5188.
37 M. H. Shao, J. H. Odell, S.-I. Choi and Y. N. Xia, *Electrochem. Commun*. **2013**, *31*, 46.
38 H. M. Song, D. H. Anjum, R. Sougrat, M. N. Hedhili and N. M. Khashab, *J. Mater. Chem.* **2012**, *22*, 25003.
39 H.-L. Liu, F. Nosheen and X. Wang, *Chem. Soc. Rev*. **2015**, *44*, 3056.
40 M. U. Khan, L. B. Wang, Z. Liu, Z. H. Gao, S. P. Wang, H. L. Li, W. B. Zhang, M. L. Wang, Z. F. Wang, C. Ma and J. Zeng, DOI: 10.1002/anie.201602512.

